SOIL

Intensive agricultural management-induced subsurface accumulation of water-extractable colloidal P in a Vertisol

Shouhao Li[1,2], **Shuiqing Chen**[1], **Shanshan Bai**[1], **Jinfang Tan**[1,2], **and Xiaoqian Jiang**[1,2]

[1]School of Agriculture, Sun Yat-sen University, Guangzhou, Guangdong, 510275, PR China
[2]Modern Agricultural Innovation Center, Henan Institute of Sun Yat-sen University, Pingyu, 463400, PR China

Correspondence: Jinfang Tan (tanjf7@mail.sysu.edu.cn) and Xiaoqian Jiang (jiangxq7@mail.sysu.edu.cn)

Abstract. Long-term excessive application of mineral fertilizer leads to phosphorus (P) accumulation, increasing the risk of P migration and loss from the soil profile. The colloids in the soil profile are important carriers for P migration due to their high P adsorption and transport capacity. It is not clearly understood how colloidal P (CP) is distributed in subsoils (< 1.2 m) of a Vertisol, contributing to subsurface P loss. Understanding the depth sequence distribution and speciation of colloidal P in the soil profile is critical for a comprehensive assessment of P loss. In this study, water-extractable colloids (WECs) with the size of 0.35–2 µm were obtained from a 0–120 cm soil profile by a sedimentation and centrifugation scheme. The dissolved reactive P (DRP) and dissolved total P (DTP) in soil supernatant with particle sizes < 0.35 µm were measured by molybdate blue colorimetry. Solution ^{31}P nuclear magnetic resonance (NMR) and P K-edge XANES (X-ray absorption near-edge structure) were used to characterize the species and distribution of CP in the soil profile of fertilized farmland. Total and available P in bulk soil and colloids decreased with soil depth. The organic P (OP) contained 97–344 mg kg^{-1} per bulk soil and 110–630 mg kg^{-1} per WEC. The OP in soil profile consists of orthophosphate mono-esters and diesters primarily according to NMR results. It suggested that OP in WECs from subsoils might be affected by the translocation of CP from surface soils, probably due to soil acidification and preferential flow caused by swelling–shrinkage clays, including montmorillonite and nontronite detected by X-ray powder diffractometer (XRD) results. Additionally, the more negative zeta potential of surface soil colloids suggests the high mobility of colloidal P towards the subsoils. The CP concentration for < 2 µm was about 38–93 mg P kg^{-1} per bulk soil, which is 6–37 times that of DRP, suggesting that CP plays a dominant role in P transport within the soil profile. The relatively small fraction of orthophosphate diesters suggests limited P assimilation by microorganisms for the accumulation of WECs containing organically bound P in subsoils. The P K-edge XANES results indicated that the proportions of Al-P, Fe-P, and inositol hexakisphosphate (IHP) of WECs decreased, but hydroxyapatite (HAP) increased with soil depth. This study showed that inorganic and organic P migrated from the surface to deeper layers along the soil profile, with soil colloids having a significant effect on P migration from both surface and subsurface layers. The findings have an important significance for soil P migration evaluation and agricultural non-point source pollution control in Vertisols.

1 Introduction

Phosphorus (P) as one of the essential macronutrients for crops is strongly immobilized with inorganic and organic soil components (Arai and Sparks, 2007). Vertisol (locally known as Shajiang black soil) covers approximately 3.13 million hectares in the Huang–Huai–Hai Plain of China (Wei et al., 2018). It is characterized by low soil organic matter (SOM), low water–air permeability, poor fertility, and strong swelling–shrinkage properties, thus contributing to low and medium crop yields (Chen et al., 2020). Therefore, high-intensity agriculture practices such as excessive fertilization have been applied for decades to maintain grain yields. Additionally, artificial ditches ($\sim$ 1–1.5 m depth) are usually dug out at the edge of the field to facilitate drainage. However, long-term excessive input of mineral fertilizers may result in considerable P accumulation in agricultural soils, and the artificial ditches bring increasing risk of P losses into surface water and groundwater, causing serious environmental issues such as outbreaks of cyanobacteria and eutrophication (Whalen and Chang, 2001; Koopmans et al., 2003; Hansen et al., 2004).

In addition to the transport of soil surface P (Pote et al., 1996), transport of soil subsurface P has also been considered to be a crucial pathway to waterways (Jorgensen and Fredericia, 1992; Kronvang et al., 1997; Xue et al., 1998; Hens and Merckx, 2001; Williams et al., 2016; Jiang et al., 2021). Some researchers have reported that high rainfall events promote the losses of P from tile drainage (1.0–1.4 m depth) (Royer et al., 2006). In previous studies in USA, colloidal P was the dominant P fraction of total P in tile water during high-rainfall events (Jiang et al., 2021). The colloids were found to carry over 1000 mg of P per kilogram, which was dominant in the transported P from subsurface soil (Jiang et al., 2021).

Currently, only a few papers have investigated dissolved and colloidal P distribution in subsoils which involved forest soils and Mollisols (Gentry et al., 2007; Wang et al., 2020; Li et al., 2022). However, the distribution of colloidal P and their speciation in the soil profile of Vertisol are still not clear. Furthermore, whether the transport of colloidal P from topsoils to subsoils occurs and contributes to total P in subsurface flow is not clearly understood. Considering the presence of abundant shrink and swell clays in Vertisol, the translocation of dissolved and colloidal P from surface soil to subsoils by preferential flow is expected to be an important P transport pathway and leads to spatial redistribution within soil profiles. Additionally, the artificial ditches could also facilitate the transport of dissolved and colloidal P from both surface and subsurface soil to surface waters, which is an important non-point source of eutrophication. Furthermore, the intensive input of fertilizer ($\sim$ 600 kg ha^{-1} compound fertilizer, N-P-K: 28-6-6) was also expected to facilitate the release of colloidal P (Liang et al., 2016).

It is expected that colloidal P could be derived from surface soils if the colloids in subsurface soil contain organic P (Li et al., 2022). The aim of this research was to explore (1) the physicochemical properties and speciation of colloidal P in the soil profile and (2) whether the colloidal organic and inorganic P exist in the subsoil and play important roles for the transport of P in intensively managed Vertisol. We assumed that the transport of colloidal P with inorganic and organic forms from the topsoil to subsoil of Vertisol is certainly possible as a result of long-term intensive agricultural management, which could bring an unavoidable risk of transport and loss of subsurface P in agricultural soil. This information is the first for the assessment of colloidal P release potential from subsoils in a Vertisol and is valuable for the construction of sustainable strategies to control agricultural P loss.

2 Materials and methods

2.1 Site description and soil sampling

The selected site was located at the agricultural study site in Pingyu County, Henan Province, China, with precipitation of 904.3 mm and a annual mean temperature of 15°, respectively. The soil is classified as a Vertisol according to the USDA Soil Taxonomy (Soil Taxonomy, USDA, 2010). Soil samples defined as A, B, C, and D were collected from four sites: Chenji Village (33°00′ N and 114°51′ E), Dingying Village (33°09′ N and 114°49′ E), Xinggang Village (32°99′ N and 114°84′ E), and Hanqiao Village (32°56′ N and 114°49′ E). Samples were taken in autumn 2021 along four vertical profiles at five or six different depths, i.e., 0–20, 20–40, 40–60, 60–80, and 80–120 cm (or 80–100 and 100–120 cm), which are denoted as depth 1, 2, 3, 4, and 5 (or 5 and 6), respectively. The cultivation system in the region involved rotating winter wheat and summer maize crops. The fertilizers for winter wheat contained 750 kg hm^{-2} compound fertilizer (N–P–K: 15–15–15) and 300 kg hm^{-2} urea. Those for summer maize included 600 kg hm^{-2} compound fertilizer and 225 kg hm^{-2} urea. The samples were air-dried, ground, and passed through a 2 mm sieve before analysis.

2.2 Physicochemical characterization of the soils

Soil pH was assessed using a pH meter with a soil-to-water ratio of 1 : 2.5. Soil total carbon (C) and nitrogen (N) levels were analyzed with an elemental analyzer (Jin et al., 2016). Total organic carbon (TOC) is measured using a TOC analyzer, which employs the combustion oxidation and non-dispersive infrared absorption method. Oxalate-extracted P (i.e., OA-P) was extracted by ammonium oxalate and oxalic acid (Jiang et al., 2015) and was considered to be the P bonded to amorphous, poorly crystalline, and organo-Fe–Al (hydr)oxides (Masiello et al., 2004; Kleber et al., 2005; Neubauer et al., 2013). The dithionite–citrate–bicarbonate

Table 1. Physicochemical characteristics of bulk soils.

Sample	Depth (cm)	pH	%TC	%TN	OC/OP	ACP ($\mu g\,g^{-1}\,h^{-1}$)	ALP ($\mu g\,g^{-1}\,h^{-1}$)	OA-P ($mg\,kg^{-1}$)	DCB-P ($mg\,kg^{-1}$)	DPS (%)
A	0–20	5.13 ± 0.04e	0.91 ± 0.00a	0.10 ± 0.00a	40.9 ± 3.4ab	647.8 ± 13.5a	465.5 ± 10.2a	142.9 ± 0.8a	178.3 ± 12.3a	4.6 ± 0.0c
	20–40	6.43 ± 0.10d	0.54 ± 0.01d	0.07 ± 0.01b	26.3 ± 2.4b	280.5 ± 4.1b	305.3 ± 14.1d	121.4 ± 5.5b	121.4 ± 5.5bc	4.4 ± 0.0c
	40–60	7.23 ± 0.02c	0.52 ± 0.00e	0.06 ± 0.01bc	30.2 ± 15.8ab	213.3 ± 6.7c	358.6 ± 4.9c	137.6 ± 6.5b	137.6 ± 6.2b	6.8 ± 0.0b
	60–80	7.52 ± 0.02b	0.67 ± 0.01c	0.06 ± 0.01bc	33.9 ± 3.8ab	127.8 ± 9.8d	390.3 ± 8.1b	31.9 ± 3.5c	98.8 ± 22.1c	6.3 ± 0.0b
	80–100	7.52 ± 0.02b	0.75 ± 0.01b	0.07 ± 0.00b	49.6 ± 5.3a	122.6 ± 11.7d	414.0 ± 11.1b	67.0 ± 6.2b	103.1 ± 16.7bc	10.0 ± 0.0a
	100–120	7.70 ± 0.02a	0.50 ± 0.01f	0.06 ± 0.01c	43.9 ± 6.7ab	96.2 ± 8.2e	346.4 ± 16.6c	75.8 ± 15.3b	100.6 ± 5.5c	7.2 ± 0.0b
B	0–20	4.88 ± 0.07e	1.17 ± 0.01a	0.14 ± 0.00a	40.2 ± 4.6a	997.2 ± 14.6a	701.4 ± 14.7a	141.70 ± 9.5a	185.9 ± 2.8a	6.5 ± 0.0c
	20–40	6.28 ± 0.02d	0.66 ± 0.01b	0.08 ± 0.00b	37.2 ± 5.1a	413.0 ± 4.7b	514.7 ± 5.8b	84.7 ± 1.3b	121.4 ± 7.8b	17.4 ± 0.0a
	40–60	7.41 ± 0.01c	0.48 ± 0.00d	0.06 ± 0.00c	26.2 ± 3.9b	186.6 ± 3.8c	509.3 ± 17.9c	59.7 ± 12.7c	66.6 ± 11.4d	16.1 ± 0.0a
	60–80	8.03 ± 0.01b	0.35 ± 0.01e	0.05 ± 0.00d	10.4 ± 1.8c	147.2 ± 14.3d	392.5 ± 16.6d	73.7 ± 3.2bc	99.8 ± 2.8c	11.0 ± 0.0b
	80–120	8.37 ± 0.01a	0.52 ± 0.01c	0.04 ± 0.00e	17.5 ± 1.4c	100.1 ± 9.3e	326.2 ± 14.3e	60.7 ± 1.9c	79.1 ± 0.9d	5.2 ± 0.0c
C	0–20	5.01 ± 0.02e	0.94 ± 0.00a	0.11 ± 0.00a	19.7 ± 2.2a	1177.6 ± 31.8a	510.6 ± 15.2b	161.7 ± 5.6a	182.3 ± 6.0a	5.3 ± 0.0c
	20–40	6.23 ± 0.03d	0.54 ± 0.00b	0.07 ± 0.00b	15.9 ± 3.0a	332.4 ± 12.8b	377.3 ± 15.3d	33.7 ± 0.7b	70.4 ± 3.90b	15.7 ± 0.0b
	40–60	7.32 ± 0.04c	0.48 ± 0.00c	0.06 ± 0.00c	9.3 ± 1.0b	190.0 ± 4.7c	578.1 ± 7.6a	29.7 ± 13.4b	45.6 ± 8.8c	19.2 ± 0.0a
	60–80	7.60 ± 0.03b	0.39 ± 0.01d	0.04 ± 0.01d	5.4 ± 0.9b	176.6 ± 3.2c	489.5 ± 4.2b	41.7 ± 6.2b	43.8 ± 5.3c	14.3 ± 0.0b
	80–120	7.74 ± 0.03a	0.27 ± 0.00e	0.04 ± 0.00d	4.9 ± 1.0b	126.8 ± 17.9d	448.1 ± 7.4c	48.7 ± 4.81b	50.1 ± 4.3c	4.8 ± 0.0c
D	0–20	5.17 ± 0.04e	0.88 ± 0.01a	0.10 ± 0.01a	28.7 ± 2.3a	749.6 ± 9.6a	502.1 ± 12.9bc	126.7 ± 6.2a	129.2 ± 6.30a	6.1 ± 0.0d
	20–40	6.97 ± 0.06d	0.57 ± 0.02b	0.07 ± 0.00b	33.1 ± 3.1a	435.4 ± 3.2b	557.2 ± 14.6a	33.7 ± 2.7b	51.4 ± 2.07b	19.4 ± 0.0ab
	40–60	7.46 ± 0.03c	0.50 ± 0.00c	0.06 ± 0.00c	32.7 ± 3.8a	136.7 ± 5.8c	526.0 ± 16.3b	34.7 ± 7.0b	65.6 ± 2.28b	21.0 ± 0.0a
	60–80	7.78 ± 0.03b	0.36 ± 0.01d	0.04 ± 0.01cd	21.1 ± 1.0b	175.9 ± 6.5d	497.1 ± 1.7c	42.7 ± 5.7b	49.8 ± 49.1c	13.7 ± 0.0c
	80–120	8.04 ± 0.01a	0.25 ± 0.00e	0.03 ± 0.01d	13.1 ± 1.7c	97.9 ± 2.3e	349.4 ± 10.3d	37.7 ± 1.7b	40.1 ± 1.93c	17.2 ± 0.0b

TC: total carbon, TN: total nitrogen, ACP: acid phosphatase activity, ALP: alkaline phosphatase activity, OA-P: oxalic-acid-extractable P, DCB-P: dithionite–citrate–bicarbonate-extracted P, DPS: degrees of phosphorus saturation (DPS=[OA-P]/0.5([OA-Fe]+[OA-Al])), OA-Fe: oxalic acid extractable Fe, OA-Al: oxalic-acid-extractable Al.

(i.e., DCB)-extracted P was extracted by sodium citrate solution, sodium hydrogen carbonate solution, and sodium dithionite (Jiang et al., 2015) and was considered to be P associated with organically bound, amorphous, and crystalline Fe oxides. The activities of acid and alkaline phosphatase, denoted as ACP and ALP, respectively, were determined by performing p-nitrophenyl phosphate assays on moist soil samples at two pH conditions, 6.5 and 11, respectively (Tabatabai et al., 1969). Soil available P was extracted with 0.5 M NaHCO$_3$ at pH 8.5 (Van Lierop, 1988) and measured by molybdate blue colorimetry (Murphy and Riley, 1962). Total inorganic P (TIP) was extracted by sulfuric acid and dilute sodium hydroxide solution separately via the sequential extraction method by Kronvang et al. (1997) and measured by molybdate blue colorimetry. For total P (TP), the extracts that were acquired from the acid and base treatments were treated with potassium persulfate and sulfuric acid before molybdate blue colorimetry, and the sum of digested extracts was defined as TP. The total organic P (TOP) was the difference between TP and TIP.

2.3 Soil particle separations and characterization of water-extractable colloids

The soil samples of A and B with different depths were fractionated by the method described by Séquaris and Lewandowsk (2003). Briefly, 100 g of soil was dispersed in 200 mL Milli-Q water in a 1 L Duran bottle and shaken for 6 h at 150 rpm. Then 600 mL Milli-Q water was added and mixed to settle. The particles > 20 and 2–20 µm were obtained by removing the supernatant after settling for 6 min and 12 h, respectively. The supernatant was subse-quently spun at $3500 \times g$ for 5 min to obtain the water-extractable colloids with size of 0.35–2 µm (calculated based on Stokes' law, and the density of the particle is assumed to be 2.65 g cm^{-3}). The final supernatant only contained the remaining fine colloids with an average hydrodynamic diameter of 351.3 ± 6.6 nm (according to dynamic light scattering (DLS) results), as well as the electrolyte phase. The dissolved reactive P (DRP) and dissolved total P (DTP) were measured by molybdate blue colorimetry (Murphy and Riley, 1962) before and after the digestion of potassium persulfate and sulfuric acid for the final supernatant.

To elucidate the inorganic and organic P species, the extracted colloidal samples after lyophilization from sample A and B with different depths were selected for the NMR analysis. The colloid samples (1 g) were mixed with 10 mL of solution containing 0.25 M NaOH and 0.05 M Na$_2$EDTA for 4 h (Jiang et al., 2017). After that, extracts were centrifuged at $10\,000 \times g$ for 30 min. The P, Fe, and Mn contents in the supernatant were measured by inductively coupled plasma optical emission spectroscopy (ICP-OES). The rest of the supernatant was freeze-dried, and then 100 mg freeze-dried extracts were dissolved in 0.1 mL D$_2$O and 0.9 mL of a solution containing 1.0 M NaOH and 0.1 M Na$_2$EDTA. After being prepared, the samples underwent centrifugation for 20 min at $10\,000 \times g$. The resulting supernatant was subsequently analyzed using a Bruker 500 MHz spectrometer with a 5 mm NMR tube. The NMR parameters contained 0.68 s acquisition time, 90° pulse width, 8000 scans, and proton decoupling. The relaxation time, which fell within the range of 3–6 s, was estimated by correlating P/(Mn+Fe) with spin-lattice relaxation times (McDowell et al., 2006). The spiking samples with myo-inositol hex-
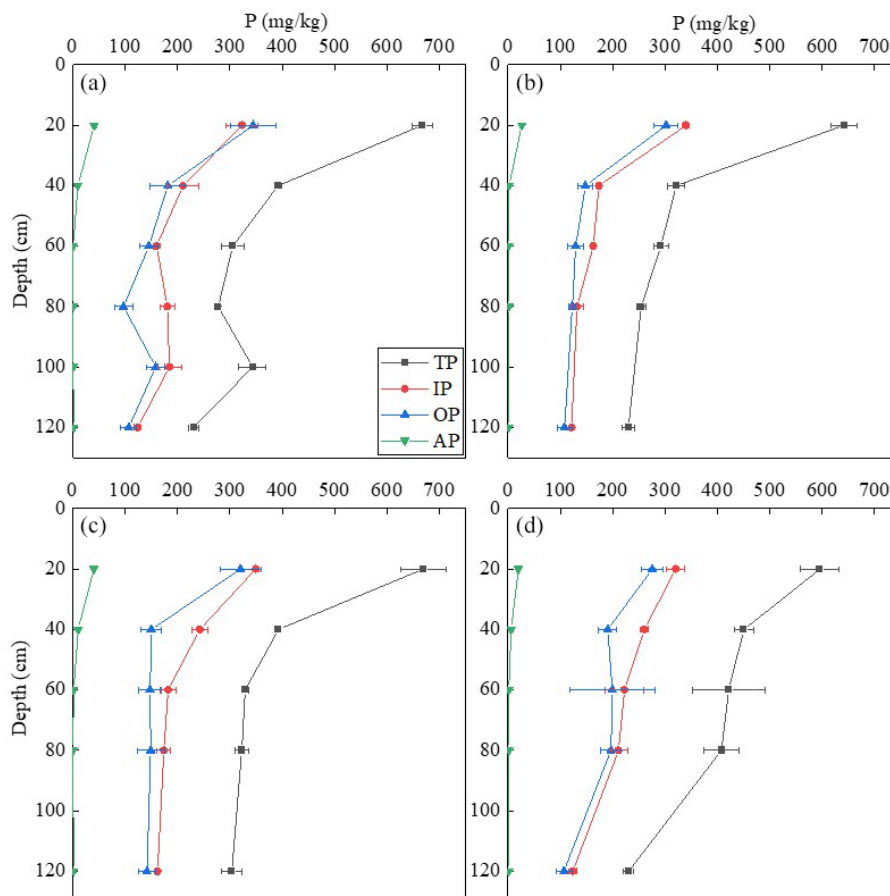
Figure 1. The concentrations of available phosphorus (AP), total phosphorus (TP), inorganic phosphorus (IP), and organic phosphorus (OP) in soil profiles of samples A, B, C, and D.

akisphosphate (myo-IHP), α- and β- glycerophosphate, and adenosine monophosphate were cited to facilitate peak identification (Bai et al., 2023). The α-, β-glycerophosphates, and mononucleotides (Glyc+nucl) were classified as orthophosphate diesters rather than to mono-esters (Young et al., 2013; Liu et al., 2018). The area under each peak was determined by integrating spectra that were processed with a line broadening of 2 and 7 Hz. MestReNova 10.0.2 software was used to process all spectra. The concentrations of individual P species were calculated by multiplying ^{31}P–NMR proportions by the total NaOH–Na$_2$EDTA-extractable P concentration. Additionally, zeta potential of colloids from sample A and B with different depths were measured using a Zetasizer (Malvern). The X-ray powder diffractometer (XRD, Empyrean) was selected to identify mineral compositions for soil colloids in the 2θ range from 3 to 90°, with a scan step size of 0.026° and a scan rate of 10° min^{-1}.

To elucidate the P bonding fractions in water-extractable colloids (WECs), the P K-edge X-ray absorptions near-edge structure (XANES) measurements were performed at Beamline 4B7A of the Beijing Synchrotron Radiation Facility, Beijing, China. The following standard samples were cho-

sen: aluminum phosphate (Al-P, AlPO$_4$), iron phosphate dihydrate (Fe-P, FePO$_4$•2H$_2$O), inositol hexakisphosphate (IHP), and hydroxyapatite (HAP, Ca$_5$(PO$_4$)$_3$OH). The soil spectra were collected using a SiLi detector in PFY (partial fluorescence yield) mode, providing detailed information about the fluorescence yield. The spectra of P standard samples were measured in total electron mode without self-absorption. Multiple spectra (three repetitions for soil samples) were collected and averaged. All XANES spectra were measured by Athena (0.9.26). The absolute energy scale was calibrated to 2149 eV (E0) as the maximum energy of the first peak in the first derivative spectrum of AlPO$_4$ (Beauchemin et al., 2003). Linear combination fitting (LCF) of the soil P spectra was conducted in the relative energy range between −10 and 30 eV. The goodness of fit was judged by the chi-squared values and R values, and P standard samples yielding the best fit were considered to be the most possible P species in the investigated soil samples.
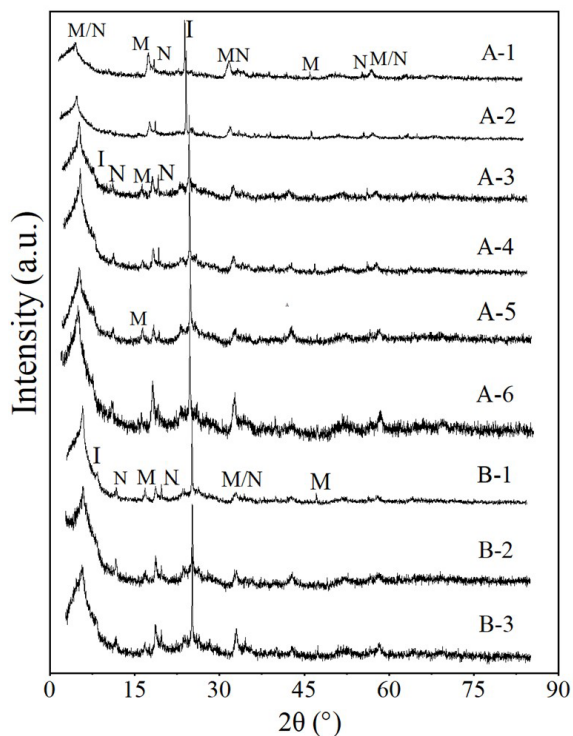
Figure 2. XRD patterns of water-extractable colloid (WEC) fractions for soil sample A and B with different depths (N: nontronite, M: montmorillonite, and I: illite).

2.4 Statistical analysis

One way analysis of variance (ANOVA) as a single-factor analysis of variance was used to test significant differences in soil indicators with different soil profiles. Tukey's honesty significance difference (HSD) test was used, and the significance level was 0.05. SPSS 25.0 and Excel software packages were used for statistical analysis. The figures were created using OriginPro 2021 (OriginLab Corp., Northampton, MA, USA).

3 Results and discussion

3.1 Physicochemical characterization and P distribution of soil profile

With the increase in soil depth in all samples, the soil pH exhibited a significant overall increase from acidic to alkaline conditions, ranging from 4.88 to 8.37 (Table 1). The serious acidity of the topsoil (0–20 cm) is probably due to increasing release of protons by nitrification processes after excessive application of nitrogen fertilizers ($750\,\mathrm{kg\,hm^{-2}}$ compound fertilizer and $300\,\mathrm{kg\,hm^{-2}}$ urea per year in the studied area) and the continuous removal of base cations by crop harvest (Guo et al., 2010). The calcareous nature of the studied soil contributed to subsoils with pH values of slight alkalinity. The contents of total C (from 1.17 % to 0.25 %)

and total N (from 0.14 % to 0.03 %) decreased significantly from topsoil to subsoil (Table 1). The accumulation of total C and N in surface soil (0–20 cm) could be related to the increased organic matter contents by biomass inputs from crop residue and N fertilization. The deepest layer of soil (80–120 cm) contained the highest pH values and the lowest total C and N contents, suggesting that the subsurface soil (20–80 cm) was also influenced by these intensive agricultural managements to some extent. The activities of acid phosphatase (ACP) were as high as $1177\,\mathrm{\mu g/(g^*h)}$ in the topsoil and decreased with the depth of the soil layer to as low as $96.2\,\mathrm{\mu g/(g^*h)}$ in the subsoil (Table 1). The activities of both acid and alkaline (ALP) phosphatase decreased significantly with depth for all the samples. The ACP was higher in the surface soil (0–20 cm) but was lower in the subsurface soil (20–120 cm) compared to ALP. Acid phosphatase activity, mainly released by plant roots and fungi, is predominant in acidic soils (Eivazi and Tabatabai, 1977; Juma and Tabatabai, 1977; Arenberg et al., 2020). Alkaline phosphatase activity, primarily produced by soil microbes, is optimized in neutral and alkaline conditions (Juma and Tabatabai, 1988; Dick et al., 2000; Krämer and Green, 2000). The higher ACP in surface soil may be attributed to an acidic pH and the rhizosphere effect, where plant roots and fungi are easily concentrated (Häussling and Marschner, 1989). Thus, lower ACP in the subsurface soil (> 20 cm) was due to increasing pH with depth.

Oxalate-extractable P concentration ranged from ∼ 30 to $162\,\mathrm{mg\,kg^{-1}}$ (∼ 7 %–45 % of TP) in all soil samples (Table 1). The oxalate-extractable P concentration in the surface soils was ∼ 127 to $162\,\mathrm{mg\,kg^{-1}}$, and it accounted for 19 %–27 % of TP and ∼ 76 % to 98 % of DCB-extractable P, suggesting that amorphous Fe–Al-oxide-bounded P was dominant for the Fe-P in the surface soils compared to crystalline Fe–Al oxides. Many studies have reported that the majority of P was associated with amorphous Fe–Al oxide fractions in many soil types (Rick and Arai, 2011; Jiang et al., 2015). It has been reported that specific anion adsorption such as P suppressed the transformation of amorphous Fe oxides to crystalline Fe oxides (Biber and Stumm, 1994), supporting the lower amount of P associated with crystalline Fe oxides.

The concentrations for TIP, TOP, and TP are included in Fig. 1. The total P concentrations in all soil samples ranged from approximately 230 to $670\,\mathrm{mg\,kg^{-1}}$ and exhibited a generally decreasing trend with the increase in soil depth (Fig. 1). TIP and TOP accounted for ∼ 48 % to 65 % and ∼ 35 % to 52 % of TP, respectively. Organic P accumulation (∼ 97 to $344\,\mathrm{mg\,kg^{-1}}$) was measured in all soil depths. The OC/OP ratio of > 200 : 1 is favorable for P immobilization (Dalal and Hallsworth, 2003; Sanyal and De Datta, 1991). The OC/OP ratio of soil samples in this study was about 4.9 to 49.6, which promoted P mineralization. Thus, the accumulation of organic P in the surface soil would be due to the increasing organic matter contents rather than the biological immobilization of P. Gradual transport of OP from

Table 2. Soil fractionation, physicochemical characteristics, and P levels of water-extracted colloids.

Sample	Depth (cm)	Soil texture	Soil sand fractions (> 20 μm, %)	Soil silt fractions (2–20 μm, %)	Colloidal fraction (0.35–2 μm, %)	Zeta potential (mV)	Colloidal P (0.35–2 μm) (mg kg soil^{-1})	DTP (< 0.35 μm, mg kg soil^{-1})	DRP (< 0.35 μm, mg kg soil^{-1})	CP/TP (%)
A	0–20	sandy loam	57.0 ± 4.0ab	34.8 ± 3.8ab	6.2 ± 0.3c	−19.1 ± 2.7	80.7 ± 3.6a	22.1 ± 1.0a	10.0 ± 1.3a	15.6 ± 1.0ab
	20–40	sandy loam	55.7 ± 1.4ab	34.2 ± 1.2ab	6.3 ± 0.3bc	−18.5 ± 1.1	51.0 ± 1.7b	15.3 ± 0.9b	7.4 ± 0.4b	13.1 ± 0.7b
	40–60	sandy loam	57.3 ± 4.5ab	33.6 ± 4.4ab	6.9 ± 0.2bc	−17.9 ± 0.6	52.4 ± 1.9b	12.3 ± 1.2c	4.6 ± 1.1c	14.4 ± 1.5b
	60–80	sandy loam	56.8 ± 2.7ab	33.0 ± 2.5ab	7.3 ± 0.6ab	−17.5 ± 2.9	52.9 ± 4.4b	6.7 ± 1.4d	2.6 ± 0.5cd	14.1 ± 1.9b
	80–100	sandy loam	59.7 ± 2.9a	30.4 ± 3.3b	7.0 ± 0.5bc	−15.7 ± 2.7	37.3 ± 1.3c	6.0 ± 0.3d	2.0 ± 0.7d	12.0 ± 0.8b
	100–120	loam	50.3 ± 1.6b	38.8 ± 0.9a	8.3 ± 0.5a	−15.8 ± 0.8	41.2 ± 1.4c	4.1 ± 0.8d	1.2 ± 0.3d	19.2 ± 1.7b
B	0–20	sandy loam	56.3 ± 3.4a	35.9 ± 3.6a	5.3 ± 0.3b	−22.0 ± 1.7	61.3 ± 2.7a	19.5 ± 1.1a	10.0 ± 1.3a	10.6 ± 1.1a
	20–40	sandy loam	56.5 ± 3.2a	34.8 ± 4.1a	5.3 ± 0.4b	−18.9 ± 1.0	31.6 ± 1.5b	14.4 ± 1.2b	6.3 ± 0.4b	10.1 ± 0.8a
	40–60	sandy loam	57.0 ± 1.9a	33.1 ± 1.2a	6.5 ± 0.3a	−9.0 ± 0.6	31.1 ± 1.1b	11.2 ± 0.9c	4.6 ± 0.3b	11.4 ± 0.7a

DTP: total P concentrations of dissolved fractions (< 0.35 μm), DRP: reactive P concentrations of dissolved fractions (< 0.35 μm), CP: colloidal P, and TP: total P.

Table 3. Concentrations of inorganic and organic P extracted by NaOH–Na$_2$EDTA (mg kg^{-1}) in the water-extractable colloid (WEC) fractions of sample A and B by solution P^{31}–NMR.

		Inorganic P (mg kg^{-1})		Organic P (mg kg^{-1})					
				Orthophosphate mono-esters				Orthophosphate diesters	
Sample	Depth (cm)	Orth	Pyro	Mono-esters*	Myo-IHP	Scyllo-IHP	Other Mono-esters	Diesters*	Glyc+nucl
A-1	0–20	202.4	10.1	50.6	8.1	3.5	39	89.1	81.0
A-2	20–40	46.8	5.1	62.0	1.4	0.0	60.6	15.4	1.8
A-3	40–60	14.1	0.14	42.2	0.6	2.0	39.6	11.4	0
A-4	60–80	14.0	0.84	38.5	0.4	0.00	38.1	0.0	0
A-5	80–100	15.3	5.5	39.6	9.2	0.00	30.4	8.1	3.5
A-6	100–120	12.5	0.0	36.3	3.8	0.00	32.5	7.5	3.8
B-1	0–20	427.5	8.6	128.3	4.3	17.6	106.4	21.4	8.5
B-2	20–40	121.0	7.3	128.1	3.7	0.00	124.4	12.2	7.3
B-3	40–60	57.5	10.4	52.9	3.5	0.00	49.4	1.7	1.7

* After diesters means calculation by including diester degradation products (i.e., Glyc+nucl: α/β- glycerophosphate, and mononucleotides) with orthophosphate diesters (Diesters) rather than orthophosphate mono-esters (Mono-esters).

the surface to subsoils could contribute to the accumulation of OP in the subsoils. Available P was very high, with ∼ 20 to 40 mg kg^{-1} in the surface soils, but it decreased dramatically with the increase in soil depth in all samples (Fig. 1). The available P content in the topsoil has been classified as high, and a threshold of 20 mg kg^{-1} has been regarded as the optimal growth level for crops (Li et al., 2015; Tang et al., 2009). This implies that the surface soils (0–20 cm) contained enough available P for the growth of winter wheat and summer maize.

3.2 Physicochemical properties of water-extracted colloids (WECs)

Considering the fact that all four samples showed similar physicochemical properties and P distributions, we further investigated the colloids of samples A and B with different depths. It is crucial to mention that the WECs are colloids that are well defined, with sizes of 0.35–2 μm operationally. The major soil series are sandy loam and loam, with a colloidal mass of 5.3 to 8.3 % (Table 2). The colloidal mass increased with depths for both samples, and previous researchers have reported a similar tendency for the recov-

ery rate of WECs in dark-colored Mollisols (Li et al., 2022). Notably, no colloids existed in at depths > 60 cm for sample B, suggesting that the generation of colloids from weathered minerals in subsoils was limited. It suggested that the colloids at a depth > 60 cm for sample A originated from the transport of upper-soil colloids mainly.

The XRD results further verified this, considering the fact that the colloids of samples A and B with all depths contained the same mineral composition (Fig. 3). The minerals in all colloids included montmorillonite, nontronite, and illite, indicating the existence of swelling–shrinkage clays. These secondary minerals all have a significant adsorption capacity for P due to great surface area and the structural binding sites of clay mineral edges (Gérard, 2016; Chen et al., 2020). Values of zeta potential for WECs were approximately −20 mV at the surface soil, but the values increased with depth (Table 2). A higher P concentration in surface soils could facilitate P special adsorption to minerals of WECs such as iron oxyhydroxide (e.g., hematite, goethite, and ferrihydrite) and aluminosilicate minerals (Arai and Sparks, 2021; Celi et al., 2001; Jiang et al., 2015), causing the surface charge to be lower compared to that of WECs in subsurface soils. The more negative values of zeta potential in the surface soil

Table 4. Phosphorus K-edge XANES fitting results showing the relative percent of each P species in water-extractable colloid (WEC) fractions (%) of sample A and B.

Sample	Depth (cm)	Al-P (%)	Fe-P (%)	HAP (%)	IHP (%)
A-1	0–20	17.0 ± 4.0	$33.0 \pm 3.0a$	$10.0 \pm 2.0c$	$32.0 \pm 6.0a$
A-2	20–40	13.0 ± 2.0	$30.0 \pm 5.0a$	$26.0 \pm 4.0bc$	$30.0 \pm 0.8ab$
A-3	40–60	14.0 ± 7.0	$28.0 \pm 0.8a$	$32.0 \pm 7.0abc$	$26.0 \pm 5.0abc$
A-4	60–80	12.0 ± 1.0	$29.0 \pm 3.0a$	$35.0 \pm 3.0abc$	$22.0 \pm 7.0abc$
A-5	80–100	11.0 ± 3.0	$24.0 \pm 3.0ab$	$45.0 \pm 2.0ab$	$10.0 \pm 0.8c$
A-6	100–120	9.0 ± 7.0	$16.0 \pm 3.0b$	$53.0 \pm 7.0a$	$13.0 \pm 5.0bc$
B-1	0–20	$25.0 \pm 7.0a$	$36.0 \pm 2.0a$	$13.0 \pm 3.0b$	17.0 ± 6.0
B-2	20–40	$11.0 \pm 0.9b$	$19.0 \pm 6.0a$	$32.0 \pm 4.0ab$	9.0 ± 4.0
B-3	40–60	$3.0 \pm 0.6b$	$20.0 \pm 5.0b$	$60.0 \pm 10.0a$	7.0 ± 4.0

Al-P: aluminum phosphate ($AlPO_4$), Fe-P: iron phosphate dihydrate ($FePO_4 \bullet 2H_2O$), HAP: hydroxyapatite ($Ca_5(PO_4)_3OH$), and IHP: inositol hexakisphosphate. Values in each column followed by the different lowercase letters indicate significant differences ($P < 0.05$).
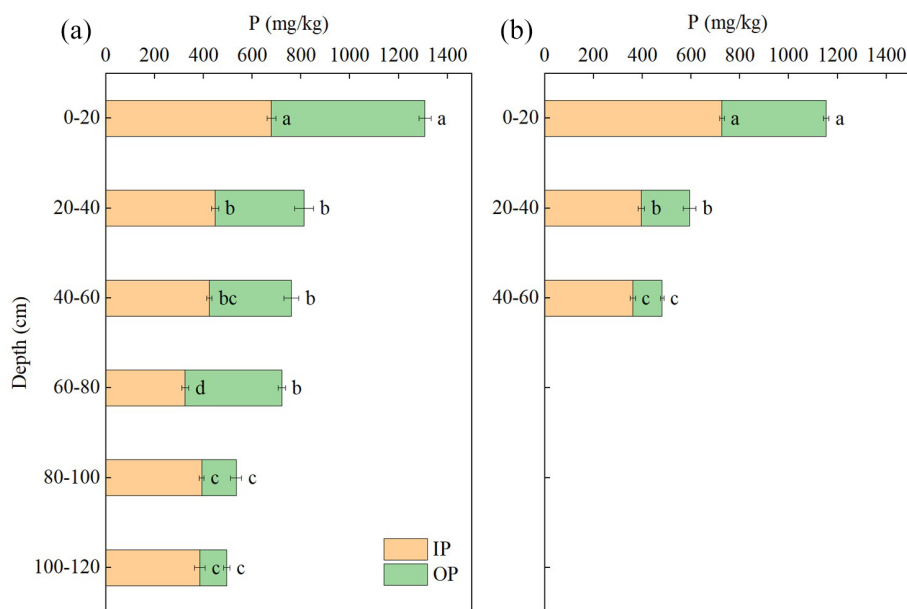
Figure 3. Inorganic (IP) and organic P (OP) concentrations ($mg\,P\,kg^{-1}$ colloids) for water-extractable colloid (WEC) fractions of sample A and B with different depths.

suggest higher mobility of colloidal P from the surface soil to the subsoils. The cation eluviation such as Ca^{2+} from the topsoil to the subsoil and the subsequent illuviation in the subsoil probably affect cation–particle interactions and contribute to the more positive zeta potential in the subsoil, as shown by the increase in hydroxyapatite with depth detected by P K-edge XANES results (see Sect. 3.4). It is important to note that DRP accounted for only 29 %–51 % of DTP (Table 2). Furthermore, the sum of colloidal P concentrations for < 0.35 µm (i.e., the difference between DTP and DRP) and 0.35–2 µm was about 38–93 mg per kilogram soil, which is 6–37 times that of DRP. It suggested that the potential contribution of CP to transport P in both surface and subsurface soil environments is important and should not be overlooked.

However, it does not exclude the transport of dissolved P with subsequent sorption to the colloidal fraction of subsoils.

3.3 Inorganic and organic P distribution in WECs with soil depth

At each sampling site, the concentration of TP in WECs was found to be the highest in the topsoil layer (0–20 cm), with a range of 1150 to 1300 $mg\,kg^{-1}$ (Fig. 3), which was significantly higher than the TP in bulk soils (~ 600–700 $mg\,kg^{-1}$). The soil colloids enriched in secondary clays such as montmorillonite, nontronite, and illite, as shown in XRD results, could readily immobilize P. Generally, the TP in WECs at each site decreased with the increase in soil depth. The con-
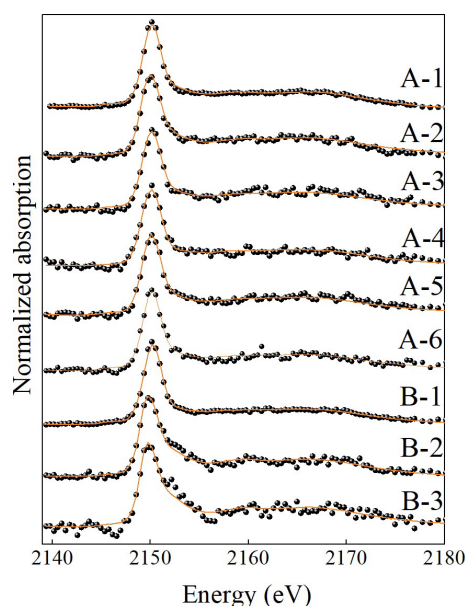
Figure 4. The results of the linear combination fitting (LCF) of the P K-edge XANES spectra for soil colloids of samples A and B. The raw data are represented by points, and the fitting results are shown by solid lines. The LCF fitting results can be found in Table 4.

centration of total IP in WECs was found to be high (ranging from 680 to 730 mg kg^{-1}) in the topsoil and displayed a decreasing trend with the increase in soil depth across all sites. As predicted, total OP concentration was high (430–630 mg kg^{-1}) in the colloids of surface soil. This is associated with the high OC concentration in the surface soil, and P was probably immobilized in the organic matter of soil. The declined tendency of OP concentrations with soil depth was probably due to the decreasing OM contents. It is noteworthy that OP was still present in the WECs of subsoils where the OC/OP was less than 300, which could not support immobilization for the accumulation of OP (Tables 1 and 3). This finding implies that colloidal-bound OP has the potential to be transported from the topsoil to subsoil layers.

3.4   Solution ^{31}P NMR analysis and P K-edge XANES analysis

The ^{31}P NMR spectroscopy spectra of WECs were presented in Table 3. It is worth mentioning that NaOH–EDTA-extracted P in the NMR analysis was below 100 %. Therefore, the concentrations of OP and IP did not correspond with the chemical digestion data presented in Fig. 2. For inorganic P, orthophosphate was found in all samples, but pyrophosphate was only found in the surface soil. Pyrophosphate was present in live fungal tissue and was easily decomposed (Koukol et al., 2008). In addition to inorganic P, the OP of WECs in all depths for samples A and B contained similar species, including orthophosphate mono-esters (36–128 mg kg^{-1}) and diesters (0–89 mg kg^{-1}) according to

NMR results (Table 3). It was clear that OP existed in colloids for both the surface and subsoils, suggesting that OP in WECs from subsoils was affected by the translocation of CP from surface soils (Li et al., 2022). Colloids containing clay minerals in the soil profile could retain orthophosphate mono-esters and diesters. Inositol phosphate has been found to be adsorbed on amorphous metal oxides and clay minerals (e.g., montmorillonite, illite, and kaolinite) (Barka and Anderson, 1962; Celi et al., 1999).

The normalized XANES spectra of WECs in samples A and B with soil profiles are shown in Table 4 and Fig. 4. Aluminum phosphate (Al-P), iron phosphate dihydrate (Fe-P), hydroxyapatite (HAP), and inositol hexakisphosphate (IHP) were detected in WECs for all the samples. The XANES results of WECs showed that the proportions of Al-P, Fe-P, and IHP of WECs decreased, but HAP increased with soil depth. As a typical alkaline soil containing carbonate concretions, the Vertisol facilitated the formation of Ca-P minerals, thus causing low P availability for crops (Westermann, 1992; Iyamuremye et al., 1996; Li et al., 2011). The decrease in soil pH in the surface soils accelerated the dissolution of Ca mineral phases, the release of associated colloidal P, and the transformation of Ca-P to Al-P and Fe-P, thus increasing the concentrations and proportions of higher-activity inorganic P fractions (Zhao et al., 2019). The dominance of hydroxyapatite in the subsoils might point to the relevance of leaching of dissolved ortho-P from topsoils into subsoils, with subsequent precipitation of apatite due to the increase in pH and Ca^{2+} concentrations. On the other hand, the dominance of hydroxyapatite in the WEC of subsoils may also reflect the presence of apatite in the unweathered parent material of soil formation. The proportions of IHP decreased with soil depth, but IHP still existed as certain amounts in the subsoil, which was further confirmed by the results of NMR.

In principle, there are four processes that could lead to the presence of organically bound colloidal P in subsoils: (i) the mobilization and subsequent transport of colloids from topsoils into subsoils, (ii) the leaching of dissolved organic P and their subsequent sorption to surfaces of WDC in subsoils, (iii) direct input of organic P into subsoils due to root exudation or root decay and their subsequent sorption to surfaces of WDC in subsoils, and (iv) the leaching of P from subsoils and its subsequent assimilation by microorganisms colonizing mineral surfaces in subsoils. As discussed above, the first process was probably dominant because more negative values of zeta potential at surface soil colloids are beneficial to the transport of colloids from the topsoil to subsoil by increasing repulsion force with soil clay particles. Additionally, the presence of abundant swelling–shrinkage clays increases preferential flow, which also facilitates the downward transport of colloids. The processes of (ii) and (iii) were also possible, but their contributions were not clear. The process of (iv) seems not to be important because the OC/OP in all soil samples ranged from 4.9 to 49.6, which did not support the immobilization of P. Additionally, microbial phosphorus

is mainly phosphate diesters (Turner et al., 2005). The relatively small fraction of orthophosphate diester indicated by ^{31}P–NMR measurements in the WEC of subsoil suggested that the process of (iv) was probably not the most relevant process explaining the accumulation of WDC containing organically bound P in subsoils.

4   Conclusions

In this study, the distribution of WECs with soil profiles (0–120 cm) was investigated in a Vertisol under high-intensity agricultural management. The P-rich WECs (0.35–2 μm) with a proportion of 5.3 %–8.3 % of bulk soil were dispersed and transported from surface soils to subsoils. The TP concentration in the WECs was as high as 1150–1300 mg kg^{-1}. It is noteworthy that OP associated with WECs was found in subsurface soils, indicating that the colloidal P was transported from surface soils to subsoils, resulting in the distribution of P-rich WECs throughout the entire soil profile. Soil colloids with a greater negative charge may be repulsed by negatively charged soil mineral surfaces, leading to the transportation of these colloidal P to the subsoil (Ilg et al., 2008). The soil acidification could facilitate deterioration of Ca-stabilized aggregates and accelerate the release of associated colloidal P. This process subsequently shifted the composition from Ca-dominated colloids to Fe–Al oxides. The existence of swelling–shrinkage minerals such as montmorillonite and nontronite promoted preferential flow and the transport of colloidal P. The sum of colloidal P < 2 μm was 6–37 times that of DRP, suggesting that colloidal P contributed to P transport significantly in the whole soil profile. Thus, it is crucial to take into account the impact of colloidal P when predicting P loss from surface to subsurface flow in Vertisol.

Data availability.   No data sets were used in this article.

Author contributions.   SL: investigation, data curation, formal analysis, writing – original draft preparation, and visualization; SC: formal analysis, data curation, and visualization; SB: formal analysis; JT: project administration; XJ: methodology, writing – reviewing and editing, project administration, and funding acquisition.

Competing interests.   The contact author has declared that none of the authors has any competing interests.

Disclaimer.   Publisher's note: Copernicus Publications remains neutral with regard to jurisdictional claims made in the text, published maps, institutional affiliations, or any other geographical representation in this paper. While Copernicus Publications makes every effort to include appropriate place names, the final responsibility lies with the authors.

Review statement.   This paper was edited by Luisella Celi and reviewed by two anonymous referees.

References

Arai, Y. J. and Sparks, D. L.: Phosphate reaction dynamics in soils and soil components: a multiscale approach, Adv. Agron., 94, 135–79, https://doi.org/10.1016/S0065-2113(06)94003-6, 2007.

Arai, Y. J. and Sparks, D. L.: Atr–Ftir spectroscopic investigation on phosphate adsorption mechanisms at the ferrihydrite–water interface, J. Colloid Interf. Sci., 241, 2317–26, https://doi.org/10.1006/jcis.2001.7773, 2021.

Arenberg, M. R., Liang, X., and Arai, Y. J.: Immobilization of agricultural phosphorus in temperate floodplain soils of illinois, USA, Biogenchemistry, 150, 257–278, https://doi.org/10.1007/s10533-020-00696-1, 2020.

Bai, S., Tan, J., Zhang, Z., Wei, M., Zhang, H., and Jiang, X.: Phosphorus speciation and colloidal phosphorus response to the cessation of fertilization in lime concretion black soil, Pedosphere, 33, 948–959, https://doi.org/10.1016/j.pedsph.2023.01.004, 2023.

Barka, T. and Anderson, P. J.: Histochemical methods for acid phosphatase using hexazonium pararosanilin as coupler, J. Histochem. Cytochem., 10, 741–753, https://doi.org/10.1177/10.6.741, 1962.

Beauchemin, S., Hesterberg, D., Chou, J., Beauchemin, M., Simard R. R., and Sayers, D. E.: Speciation of phosphorus in phosphorus-enriched agricultural soils using x-ray absorption near-edge structure spectroscopy and chemical fractionation, J. Environ. Qual., 32, 1809–1819, https://doi.org/10.2134/jeq2003.1809, 2003.

Biber, M. V. and Stumm, W.: An in-situ atr-ftir study: the surface coordination of salicylic acid on aluminum and iron (iii) oxides, Environ. Sci. Technol., 28, 763–768, https://doi.org/10.1021/es00054a004, 1994.

Celi, L., Lamacchia, S., Marsan, F. A., and Barberis, E.: Interaction of inositol hexaphosphate on clays: adsorption and charging phenomena, Soil Sci., 164, 574–585, https://doi.org/10.1097/00010694-199908000-0000, 1999.

Celi, L. Presta, M., Ajmore-Marsan, F., and Barberis, E.: Effects of pH and electrolytes on inositol hexaphosphate interaction with goethite, Soil Sci. Soc. Am. J., 65, 753–760, https://doi.org/10.2136/sssaj2001.653753x, 2001.

Chen, L., Li, F., Li, W., Ning, Q., Li, J., Zhang, J., Ma, D., and Zhang, C.: Organic amendment mitigates the negative impacts of mineral fertilization on bacterial communi-

ties in Shajiang black soil, Appl. Soil Ecol., 150, 103457, https://doi.org/10.1016/j.apsoil.2019.103457, 2020.

Dalal, R. C. and Hallsworth, E. G.: Measurement of isotopic exchangeable soil phosphorus and interrelationship among parameters of quantity, intensity and capacity factors, Soil Sci. Soc. Am. J., 41, 8186, https://doi.org/10.2136/sssaj1977.03615995004100010025x, 2003.

Dick, W. A., Cheng, L., and Wang, P.: Soil acid and alkaline phosphatase activity as ph adjustment indicators, Soil Biol. Biochem., 32, 1915–1919, https://doi.org/10.1016/S0038-0717(00)00166-8, 2000.

Eivazi, F. and Tabatabai, M. A.: Phosphatases in soils, Soil Biol. Biochem., 9, 167–172, https://doi.org/10.1016/0038-0717(77)90070-0, 1977.

Gentry, L. E., David, M. B., Royer, T. V., Mitchell, C. A., and Starks, K. M.: Phosphorus transport pathways to streams in tile-drained agricultural watersheds, J. Environ. Qual., 36, 408–415, https://doi.org/10.2134/jeq2006.0098, 2007.

Gérard, F.: Clay minerals, iron/aluminum oxides, and their contribution to phosphate sorption in soils–a myth revisited, Geoderma, 262, 213–226, https://doi.org/10.1016/j.geoderma.2015.08.036, 2016.

Guo, J. H., Liu, X. J., Zhang, Y., Shen, J. L., Han, W. X., Zhang, W. F., Christie, P., Goulding, K. W. T., Vitousek, P. M., and Zhang, F. S.: Significant acidification in major Chinese croplands, Science, 327, 5968, https://doi.org/10.1016/j.scitotenv.2017.09.289, 2010.

Hansen, J. C., Cade-Menun, B, J., and Strawn, D. G.: Phosphorus speciation in manure amended alkaline soils, J. Environ. Qual., 33, 1521–1527, https://doi.org/10.2134/jeq2004.1521, 2004.

Häussling, M. and Marschner, H.: Organic and inorganic soil phosphates and acid phosphatase activity in the rhizosphere of 80-year-old norway spruce [picea abies (l.) karst.] trees, Biol. Fert. Soils, 8, 128–133, https://doi.org/10.1007/bf00257756, 1989.

Hens, M. and Merckx, R.: Functional characterization of colloidal phosphorus species in the soil solution of sandy soils, Environ. Sci. Technol., 35, 493–500, https://doi.org/10.1021/es0013576, 2001.

Ilg, K., Dominik, P., Kaupenjohann, M., and Siemens, J.: Phosphorus-induced mobilization of colloids:model systems and soils, Eur. J. Soil Sci., 59, 233–246, https://doi.org/10.1111/j.1365-2389.2007.00982.x, 2008.

Iyamuremye, F, Dick, R. P., and Baham, J.: Organic amendments and phosphorus dynamics: ii. distribution of soil phosphorus fractions, Soil Sci., 161, 436–443, https://doi.org/10.1097/00010694-199607000-00003, 1996.

Jiang, X., Bol, R., Willbold, S., Vereecken, H., and Klumpp, E.: Speciation and distribution of P associated with Fe and Al oxides in aggregate-sized fraction of an arable soil, Biogeosciences, 12, 6443–6452, https://doi.org/10.5194/bg-12-6443-2015, 2015.

Jiang, X., Amelung, W., Cade-Menun, B. J., Bol, R., Willbold, S., Cao, Z., and Klumpp, E.: Soil organic phosphorus transformations during 2000 years of paddy-rice and non-paddy management in the Yangtze River Delta, China, Sci. Rep.-UK., 7, 1–12, https://doi.org/10.1016/j.geoderma.2022.116296, 2017.

Jiang, X., Livi, K. J. T., Arenberg, M, R., Chen, A., Chen, K., Gentry, L., Li, Z., Xu, S., and Arai, Y.: High flow event induced the subsurface transport of particulate phosphorus and its speciation in agricultural tile drainage system, Chemosphere, 263, 128147, https://doi.org/10.1016/j.chemosphere.2020.128147, 2021.

Jin, Y., Liang, X., He, M., Liu, Y., Tian, G., and Shi, J.: Manure biochar influence upon soil properties, phosphorus distribution and phosphatase activities: a microcosm incubation study, Chemosphere, 142, 12844, https://doi.org/10.1016/j.chemosphere.2015.07.015, 2016.

Jorgensen, P. R. and Fredericia, J.: Migration of nutrients, pesticides and heavy metals in fractured, Geotechnique, 42, 67–77, https://doi.org/10.1016/0148-9062(92)91738-q, 1992.

Juma, N. G. and Tabatabai, M. A.: Effects of trace elements on phosphatase activity in soils, Soil Sci. Soc. Am. J., 41, 343–346, https://doi.org/10.2136/sssaj1977.03615995004100020034x, 1977.

Juma, N. G. and Tabatabai, M. A.: Phosphatase activity in corn and soybean roots: conditions for assay and effects of metals, Plant Soil, 107, 39–47, 1988.

Kleber, M., Mikutta, R., Torn, M., and Jahn, R.: Poorly crystalline mineral phases protect organic matter in acid subsoil horizons, Eur. J. Soil Sci., 56, 717–725, https://doi.org/10.1016/j.geoderma.2004.12.018, 2005.

Koopmans, G. F., Chardon, W. J., Dolfing, J., Oenema, O., Van der Meer, P., and Riemsdijk, W. V.: Wet chemical and phosphorus-31 nuclear magnetic resonance analysis of phosphorus speciation in a sandy soil receiving long-term fertilizer or animal manure applications, J. Environ. Qual., 32, 287–295, https://doi.org/10.2134/jeq2003.0287, 2003.

Koukol, O., Beňová, B., Vosmanská, M., Frantík, T., Vosátka, M., and Kovářová, M.: Decomposition of spruce litter needles of different quality by setulipes androsaceus and thysanophora penicillioides, Plant Soil., 311, 151–159, https://doi.org/10.1007/s11104-008-9666-5, 2008.

Krämer, S. and Green, D. M.: Acid and alkaline phosphatase dynamics and their relationship to soil microclimate in a semiarid woodland, Soil Biol. Biochem., 32, 179–188, https://doi.org/10.1016/S0038-0717(99)00140-6, 2000.

Kronvang, B., Anker, L., and Ruth, G.: Suspended sediment and particulate phosphorus transport and delivery pathways in an Arable Catchment, Gelbaek Stream, Denmark, Hydrol. Process., 11, 627–642, 1977.

Kronvang, B., Grant, R., and Laubel, A. L.: Sediment and phosphorus export from a lowland catchment: quantification of sources, Water Air Soil Poll., 99, 465–476, 1997.

Li, D., Zhang, G., and Gong, Z.: On taxonomy of Shajiang black soils in China, Soils, 43, 623-629, https://doi.org/10.13758/j.cnki.tr.2011.04.015, 2011.

Li, H., Liu, J., Li, G., Shen, J., Bergström, L., and Zhang, F.: Past, present, and future use of phosphorus in chinese agriculture and its influence on phosphorus losses, Ambio, 44, 274–285, https://doi.org/10.1007/s13280-015-0633-0, 2015.

Li, Y., Livi, K. J. T., Arenberg, M. R., Xu, S. W., and Arai, Y.: Depth sequence distribution of water extractable colloidal phosphorus and its phosphorus speciation in intensively managed agricultural soils, Chemosphere, 286, 131665, https://doi.org/10.1016/j.chemosphere.2021.131665, 2022.

Liang, X., Jin, Y., Zhao, Y., Wang, Z., Yin, R., and Tian, G.: Release and migration of colloidal phosphorus from a typical agricultural field under long-term phosphorus fertiliza-

tion in southeastern china, J. Soil Sediment., 16, 842–853, https://doi.org/10.1007/s11368-015-1290-4, 2016.

Liu, J., Cade-Menun, B. J., Yang, J., Hu, Y., Liu, C, W., Tremblay, J., LaForge, K., and Bainard, L. D.: Long-term land use affects phosphorus speciation and the composition of phosphorus cycling genes in agricultural soils, Front. Microbiol., 9, 1643, https://doi.org/10.3389/fmicb.2018.01643, 2018.

Masiello, C. A., Chadwick, O. A., Southon, J., Torn, M. S., and Harden, J. W.: Weathering controls on mechanisms of carbon storage in grassland soils, Global Biogeochem. Cy., 18, 0886-6236, https://doi.org/10.1029/2004GB002219, 2004.

McDowell, R. W., Stewart, I., and Cade-Menun, B: An examination of spin–lattice relaxation times for analysis of soil and manure extracts by liquid state phosphorus-31 nuclear magnetic resonance spectroscopy, J. Environ. Qual., 35, 293–302, https://doi.org/10.2134/jeq2005.0285, 2006.

Murphy, J. and Riley, J. P.: A modified single solution method for the determination of phosphate in natural waters, Anal. Chim. Acta, 27, 31–36, https://doi.org/10.1016/s0003-2670(00)88444-5, 1962.

Neubauer, E., Schenkeveld, W. D. C., Plathe, K. L., Rentenberger, C., Von Der Kammer, F., Kraemer, S. M., and Hofmann, T.: The influence of ph on iron speciation in podzol extracts: iron complexes with natural organic matter, and iron mineral nanoparticles, Sci. Total Enviroon., 461, 108-116, https://doi.org/10.1016/j.scitotenv.2013.04.076, 2013.

Pote, D. H., Daniel, T, C., Moore, P. A., Nichols, D. J., Sharpley, A. N., and Edwards, D. R.: Relating extractable soil phosphorus to phosphorus losses in runoff, Soil. Sci. Soc. Am. J., 60, 855–859, https://doi.org/10.2136/sssaj1996.03615995006000030025x, 1996.

Rick, A. R. and Arai, Y.: Role of natural nanoparticles in phosphorus transport processes in ultisols, Soil. Sci. Soc. Am. J., 75, 335–347, https://doi.org/10.2136/sssaj2010.0124nps, 2011.

Royer, T. V., David, M. B., and Gentry, L. E.: Timing of riverine export of nitrate and phosphorus from agricultural watersheds in illinois: implications for reducing nutrient loading to the Mississippi River, Environ. Sci. Technol., 40, 4126–4131, https://doi.org/10.1021/es052573n, 2006.

Sanyal, S. K. and De Datta, S. K.: Chemistry of phosphorus transformations in soil, Advances in Soil Science, 1–120, Springer, https://doi.org/10.1007/978-1-4612-3144-8, 1991.

Séquaris, J. M. and Lewandowsk, H.: Physicochemical characterization of potential colloids from agricultural topsoils, Physicochemical and Engineering Aspects Colloid Surface A, 217, 93–99, https://doi.org/10.1016/S0927-7757(02)00563-0, 2003.

Soil Taxonomy, USDA: Soil survey staff, keys to soil taxonomy, USDA-Natural Resources Conservation Service, Washington, DC, 2010.

Tabatabai, M. A. and Bremner, J. M.: Use of p-nitrophenyl phosphate for assay of soil phosphatase activity, Soil Biol. Biochem., 1, 301–307, https://doi.org/10.1016/0038-0717(69)90012-1, 1969.

Tang, X., Ma, Y., Hao, X., Li, X., Li, J., Huang, S., and Yang, X.: Determining critical values of soil olsen-p for maize and winter wheat from long-term experiments in china, Plant Soil, 323, 143–151, https://doi.org/10.1007/s11104-009-9919-y, 2009.

Turner, B. L., Cade-Menun, B. J., Condron, L. M., and Newman, S: Extraction of soil organic phosphorus, Talanta, 66, 294–306, https://doi.org10.1016/j.talanta.2004.11.012, 2005.

van Lierop, W.: Determination of available phosphorus in acid and calcareous soils with the Kelowna multiple-elementextractant, Soil Sci., 146, 284, https://doi.org/10.1097/00010694-198810000-00009, 1988.

Wang, L., Missong, A., Amelung, W., Willbold, S., Prietzel, J., and Klumpp, E.: Dissolved and colloidal phosphorus affect P cycling in calcareous forest soils, Geoderma, 375, 114507, https://doi.org/10.1016/j.geoderma.2020.114507, 2020.

Wei, C., Gao, W., William, R., and Li, B.: Shrinkage characteristics of lime concretion black soil as affected by biochar amendment, Pedosphere, 28, 713–725, https://doi.org/10.1016/S1002-0160(18)60041-4, 2018.

Westermann, D. T.: Lime effects on phosphorus availability in a calcareous soil, Soil Sci. Soc. Am. J., 56, 489–494, https://doi.org/10.2136/sssaj1992.03615995005600020024x, 1992.

Whalen, J. K. and Chang, C.: Phosphorus accumulation in cultivated soils from long-term annual applications of cattle feedlot manure, J. Environ. Qual., 30, 229–237, https://doi.org/10.2134/jeq2001.301229x, 2001.

Williams, M, R., King, K, W., Ford, W., Buda, A. R., and Kennedy, C. D.: Effect of tillage on macropore flow and phosphorus transport to tile drains, Water. Resour. Res., 52, 2868–2882, https://doi.org/10.1002/2015WR017650, 2016.

WRB: Iwg. World Reference Base for Soil Resources: International soil classification system for naming soils and creating legends for soil maps, ISSN 0532-0488, 2014.

Xue, Y., David, M. B., Gentry, L. E., and Kovacic, D. A.: Kinetics and Modeling of Dissolved Phosphorus Export from a Tile-Drained Agricultural Watershed, J. Environ. Qual., 27, 917–922, https://doi.org/10.2134/jeq1999.00472425002800030048x, 1998.

Young, E. O., Ross, D. S., Cade-Menun, B. J., and Liu, C. W.: Phosphorus speciation in riparian soils, a phosphorus-31 nuclear magnetic resonance spectroscopy and enzyme hydrolysis study, Soil. Sci. Soc. Am. J., 77, 1636–1647, https://doi.org/10.2136/sssaj2012.0313, 2013.

Zhao, F., Zhang, Y., Dijkstra, F. A., Li, Z., Zhang, Y., Zhang, T., Lu, Y., Shi, J., and Yang, L.: Effects of amendments on phosphorous status in soils with different phosphorous levels, Catena, 172, 97–103, https://doi.org/10.1016/j.catena.2018.08.016, 2019.